International Journal of Concrete Structures and Materials

RESEARCH

Open Access

New Anchorage Technique for GFRP Flexural Strengthening of Concrete Beams Using Bolts-End Anchoring System

Djarir Yahiaoui[1*], Abdelaziz Boutrid[2,3], Mohamed Saadi[1], Belgacem Mamen[2] and Tayeb Bouzid[1]

Abstract

The concept of external glass FRP composite confinement is a current process for strengthening concrete beams subjected to static loads. End anchorage glass FRP composites of 80 mm width and 90–130 mm length with different thicknesses (2.4 and 4.8 mm) have been fixed at the bottom of beams with bolts of various diameters (6 and 10 mm). For this purpose, the behavior of beams strengthened with bolt-end anchoring glass fiber polymer composites (BEGFPC) has been analyzed. It is concluded that the load capacity of the BEGFPC beams is improved by increasing the end-anchorage glass FRP composite thickness (about 98–188%). In addition, the BEGFPC system with bolts of 6 mm diameter has significantly improved the flexibility of beams. In contrast, the 10 mm bolts in diameter give a high ultimate load, whatever their quantity. Therefore, combining bolts with diameters of 6 and 10 mm would be the best solution for increasing the ultimate load and ductility of the retrofitted beams. Depending on the number and bolts' arrangement, there is also an enhancement in the crack patterns by changing from intermediate flexural failure to shear failure in beams.

Keywords Tension zone, Bolts-end anchoring, Glass FRP, Bolts, Crack patterns, Failure modes

1 Introduction

Strengthening and rehabilitating degraded concrete structures by external bonding is a fruitful technique. Steel plates are popular due to their high strength, flexibility, and homogenous characteristics (Alasadi et al., 2019). However, steel plates corrode and lose thickness if exposed to open environments. Significantly, the influence of corrosion is limited by covering the concrete parts with anti-corrosive compounds, such as carbon fiber reinforced polymer (CFRP), glass FRP, aramid FRP, and basalt FRP (Al-Hamrani & Alnahhal, 2019; Norooz Olyaee & Mostofinejad, 2019; Yahiaoui et al., 2022). These FRPs are available in rebar, laminate, or sheet form. More importantly, the FRPs are lightweight, strong, and more cost-effective components to manufacture than metal plates. Therefore, the external FRPs bonding process has been widely used to strengthen concrete beams, because it makes the material more ductile (El Ghadioui et al., 2022; Pavithra et al., 2022). Prior studies reported that the FRP composites remained elastic until brittle debonding or FRP failure occurred (Salama et al., 2019; Zhou et al., 2018).

The effects of fiber direction and reinforcement ratio of glass fiber reinforced polymer (GFRP) sheets have been analyzed to examine the behavior of concrete beams. It is reported that the GFRP sheets strengthen the beam and improve the flexural deflection of the

Journal information: ISSN 1976-0485 / eISSN 2234-1315

*Correspondence:
Djarir Yahiaoui
d.yahiaoui@univ-batna2.dz
[1] LGC-ROI, Civil Engineering Laboratory-Risks and Structures in Interactions, Department of Civil Engineering, Faculty of Technology, University of Batna 2, 05001 Batna, Algeria
[2] Department of Civil Engineering, Faculty of Science and Technology, Abbès Laghrour University, 40000 Khenchela, Algeria
[3] Mineral Processing and Environmental Laboratory, Department of Mines, Badji Mokhtar University, 23000 Annaba, Algeria

Springer Open

© The Author(s) 2023. **Open Access** This article is licensed under a Creative Commons Attribution 4.0 International License, which permits use, sharing, adaptation, distribution and reproduction in any medium or format, as long as you give appropriate credit to the original author(s) and the source, provide a link to the Creative Commons licence, and indicate if changes were made. The images or other third party material in this article are included in the article's Creative Commons licence, unless indicated otherwise in a credit line to the material. If material is not included in the article's Creative Commons licence and your intended use is not permitted by statutory regulation or exceeds the permitted use, you will need to obtain permission directly from the copyright holder. To view a copy of this licence, visit http://creativecommons.org/licenses/by/4.0/.

beams (Sankaramoorthy et al., 2022). Furthermore, many researchers recommended using hybrid FRP composites, including diverse kinds of fiber sheets, to enhance the efficiency of such strengthening processes. This design would cause the failure to occur at different strains of the sheets under loading, allowing the composites to fail gradually and thereby enhancing the flexibility of the strengthened element (Vahidpour et al., 2022). Various flexural tests have been performed on hybrid CFRP/GFRP-concrete beams with CFRP layers in flanges. The optimal volume percentage of carbon fiber was determined to be 25–33% (Nguyen et al., 2015). Additional research conducted an experimental assessment of strengthened concrete beams by various combinations, including carbon-glass fabric and vegetable fiber. It is revealed that all reinforced beams provide superior characteristics to the controlled beam, with significant bending loading improvements (Djeddi et al., 2016).

Glass fiber Reinforced polymer can also be used to rehabilitate reinforced concrete (RC), pre-stressed concrete (PC), and metallic and masonry structures. Sharma et al. (2022) suggested a non-destructive health monitoring strategy for steel-reinforced and GFRP-reinforced concrete beams using a judicious combination of advanced non-destructive techniques of Acoustic Emission (AE) and optical technique of Digital Image Correlation (DIC). AE has been used to characterize the onset and propagation of the cracking pattern and mode of failure in the beams. On the other hand, DIC aided in visualizing strain fields by comparing subsequent pictures of a speckle pattern on the surface of the RC beams. The information provided by DIC would help validate AE observations, as visible changes in the strain field could correlate well with the AE emissions recorded. When used in combination, the damage monitoring tools successfully give a progression of damage leading to failure in steel and GFRP-reinforced concrete beams. Integrated the two NDT (non-destructive testing) monitoring tools for fracture analysis of differently reinforced concrete beams involving steel and GFRP bars as reinforcement alternatives. Acoustic emission can monitor the structure in terms of volumetric and surface effects. However, with limited visualization accuracy, DIC detects deformations and provides full-field displacement maps, although only on the surface of the monitored specimen. Therefore, integrating these two techniques can lead to more quantitative and comprehensive non-destructive monitoring tools compared to the stand-alone use of each method in RC structures. It is successfully demonstrated that combined AE and DIC monitoring enhance non-destructive monitoring skills in RC structures and effectively depict their cracking behavior. Garhwal et al. (2021) investigated the flexural behavior of glass fiber reinforced polymer (GFRP) repaired reinforced beams. A novel methodology has been developed for assessing the performance of these beams using AE techniques. This approach facilitates non-destructive evaluation of FRP-repaired RC structures with a prior indication of their damage post-repair.

Structural performance of FRP-retrofitted RC beams under combined loading has been largely investigated in the existing literature. Amini Pishro et al., (2022a, 2022b) analyzed numerically unreinforced and FRP-retrofitted RC beams subjected to bending and torsion. The synchronized effects of such solicitations and the strengthening effects of FRP on the behavior of these RC beams have been well-reported. Accordingly, an ANN model was used to calculate the structural behavior of FRP-confined RC beams. The model and trial results confirmed that this numerical simulation had relatively good accuracy in predicting the structural behavior of retrofitted RC beams under combined loading. Furthermore, the structural behavior of RC T-beams, strengthened by externally bonded carbon fiber reinforced polymers (CFRPs), subjected to combined solicitations has been analyzed by Amini Pishro et al., (2022a, 2022b). Based on their previous research, the FEM software ABAQUS has been applied to adjust the experimental results of scaled RC beams. There is no precise analytical equation to control the behavior of EB-FRP-strengthened RC T-beams under combined solicitations. For this purpose, an Artificial Neural Network (ANN) has been developed and trained to evaluate such elements' structural responses and effectiveness. The results were verified based on the methods of Mean Square Error (MSE) and Multiple Determination Coefficients. The ACI-440 in the SNI Beton Indonesia code does not contain a formula that calculates the shear increase in concrete caused by the increase in the bending moment due to FRP strengthening. Therefore, Tudjono et al. (2015) assessed the improvement in the capacity of concrete beams bound with a combination of FRP flexural and U-shaped shear strengthening. Pishro and Feng (2017) reported exciting conclusions about the behavior of reinforced concrete beams strengthened with bonded FRP sheets subjected to torsion, shear, and flexure. This was presented by analyzing the existing literature. The outcomes have been deeply explored. Furthermore, modeling and numerical simulations have been developed to improve the resistance of RC beams reinforced with externally bonded FRP.

Another way to reduce excessive delamination of the FRP from the concrete is to use anchors that provide a continuous load path. Recently, the behavior and capacity of FRP anchors have received research attention (Ali et al., 2022; Del Rey Castillo et al., 2018; Mhanna et al., 2021). Several anchorage systems have been established (2018b;

Chen et al., 2018a; Esmaeili et al., 2022; Zhou et al., 2017), although FRP U-anchors have often been effective compared to other anchoring devices (2018b; Chen et al., 2018a; Zhang et al., 2021). However, the placement of FRP U-jacket anchors throughout the span to prevent plate-end debonding mechanism may not be an operative method to improve the effectiveness of FRP strengthening applications, as additional materials are required to reach a specified strength.

Based on the existing literature, reinforced structures subjected to uniaxial compression loading present a ductile failure compared to bending loading. Meanwhile, the corresponding failure is brittle and dangerous for reinforced beams loaded in such a way. It frequently occurs at the lower beam side because of tensile stress. The application of carbon (CFRP), aramid (AFRP), and glass (GFRP) for strengthening beams has been wildly investigated by various researchers. However, the testing data on the flexural response of beams reinforced with bolt-end anchoring glass fiber polymer composites (BEGFPC) is limited, Tran et al. (2022). More testing data on (BEGFPC) strengthening is desired to supplement the current understanding for more reliable and convincing results. The efficacy of beam strengthening using (BEGFPC) has not been compared yet. In addition, the design guidelines provided in ACI 440.2R-08 (American Concrete Institute, 2008) are applicable for CFRP/GFRP/AFRP materials. At the same time, the applicability of bolt-end anchoring to strengthen RC structure has not yet been verified. The verification of the predictions on (BEGFPC) strengthening is thus desired.

Therefore, this work proposes a performed design process for the flexural behavior of beams with bolt-end anchoring glass fiber polymer composites (BEGFPC). Furthermore, the present study evaluates the effect of the BEGFRPC layer thickness, bolts diameter, and its arrangement on the flexural performance and bonding behavior of concrete beams externally strengthening under three-point loading. Twenty-two beams are divided into three series and were tested. The beam control is strengthened only in flexure with a GFRP sheet of 2.4 mm thickness. The second series of beams are reinforced with a GFRP sheet and bolts. The third series of beams is strengthened with a GFRP sheet and bolts-end anchoring GFRP with different thicknesses (2.4 and 4.8 mm). The experimental results incorporate load versus mid-span deflection response curve, elastic stiffness, ultimate loads and flexural capacity, energy absorption capacity, and associated failure mode of the tested beams.

2 Experimental Program

This section presents the different materials' mechanical properties, the test setup description, and the procedures used to investigate the bond properties.

2.1 Materials

2.1.1 Concrete

The concrete mix is prepared with Ordinary Portland cement. The mixture is designed to reach an average compressive strength of 25–30 MPa at 28 days. It is elaborated using a water/cement ratio of 0.57, according to the ACI-211.1-91 design procedure (ACI211.1, 2009). The effect of fine and coarse aggregates has been considered, as reported by (Nili et al., 2017). The mix is cast into ($150 \times 150 \times 150$ mm) molds for compression testing. Then, the samples are tested after 28 days to measure compressive strength according to (ASTM C39/C39M-17b, 2017). The average compressive strength after 28 days is 25 MPa, Table 1.

2.1.2 Glass Fiber Reinforced Polymer

Local polyester resin and bidirectional fiber-glass are used to develop a low-cost glass fiber-reinforced polymer composite, as shown in Fig. 1.

In the boating industry, this category of bi-directional fiber-glass is commonly used. For strengthening GFRC beams, glass FRP composites were prepared and tested

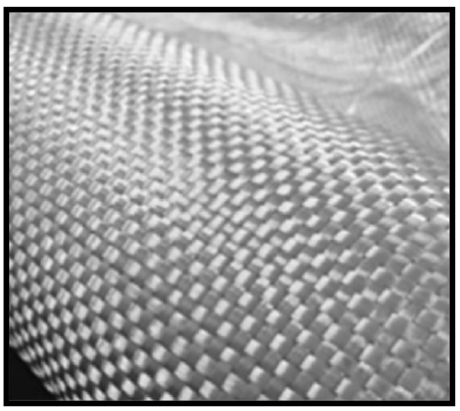

Fig. 1 Bi-directional glass fiber reinforced polymer (GFRP)

Table 1 Mix proportion of the C25 concrete

Material	Cement (kg/m^3)	Sand (kg/m^3)	Coarse aggregate (kg/m^3)	Fine aggregate (kg/m^3)	Water (kg/m^3)	Superplasticizer (% cement weight)	Compressive Strength (MPa)
	400	773	496	496	163	0.9–1.1	25

using the UTS-SHIMADZU universal machine according to the standard guidelines of (ASTM D638-10, 2010). Three tensile samples of FRP Composite were tested to obtain accurate results, as shown in Table 2.

2.2 Specimen and Anchoring System

As mentioned, the mixture is cast into ($500 \times 150 \times 150$ mm) molds for three-point testing. First, the beam specimens are demolded after 24 h from casting and left in a controlled environment at a temperature of 20 °C and relative humidity of 100% for 28 days. Then, the polyester resin is applied to the sample's external surface with a brush. Then, a resin-soaked fiberglass board is covered at the bottom of the concrete beam. The concrete surface is adequately cleaned to remove dust before applying the GFRP compound. The last strengthened specimen is shown in Fig. 2a.

To increase the bonding between the GFRP sheets and the concrete beam, the GFRP anchor plates are connected to the bottom by bolts, as shown in Fig. 2c, b. In addition, the reason for using anchoring plates with different thicknesses at the bottom of the beam is to distribute the stresses generated from the bolts on the concrete surface. The dimensions and location of holes for the plates (1, 2, 3, 4, and 5) are shown in Fig. 2d. Moreover, the diameters of the bolts are 6 and 10 mm. The beams' designations summary and the parameters of investigation are presented in Table 3 and Fig. 3.

2.3 Test Setup

According to (ASTM D7958/D7958M, 2017), three-point bending tests are performed, as shown in Fig. 3. The tests are conducted through universal test equipment with a load capacity of 200 kN. Quasi-static loading is a process in which the vertical displacement of the beam change infinitely slowly; thus, the system appears nearly static. It is an ideal process that is reversible and experiences equilibrium at every test stage. Therefore, the displacement rate is controlled at 0.05 mm/min for GFRP-strengthened beams. The load is registered during the entire test with the integrated load sensor of the test equipment. At the same time, the deflection of the control point is monitored using a linear variable displacement transducer (LVDT) which is rigidly attached to the roller used for the load application. The tests were stopped when the load applied after achieving the peak load was about 20% of the ultimate load.

Table 2 Mechanical properties of epoxy resin and GFRP composite

FRP Composite	Tensile stress (MPa)	Ultimate strain (%)	Modulus of elasticity (GPa)	Standard deviation
Epoxy resin	17.20	0.6322	2.72	1.08
GFRP	377.64	2.04%	43	1.91

3 Experimental Results

3.1 Load–Deflection Relationship

The load versus deflection results are shown in Figs. 4, 5 and 6 for all beams. The curves are used to assess the effect of the end-anchorage GFRP thickness, the number, the position, and the diameter of the bolts. Compared with specimen 0B-1C, a more extended elastic stage and a higher stiffness are presented with the inclusion of the end-anchorage system GFRP. The typical load–deflection relationships are divided into three types of curves.

Initially, the first type is described in specimen 0B-1C. When the load increases linearly up to 23 kN, it drops sharply, because the interface is deboning to the beam.

The second type presents a substantial augmentation in the applied load; of about 90%, 104%, and 127% in beams 2B-1C-D10, 4B-H-1C-D10, 4B-V-1C-D10, 2B-2C-D10 and 2B-3C-D10, respectively. Afterward, the load suddenly decreases until it reaches about 12–20 KN. This is because the GFRP sheet separates from the beam in the middle. Then, it goes back to increase until it arrives at 22.5 kN, 30 kN, 35 kN, 40 kN, and 50 kN for beams 2B-1C, 4B-H-1C, 4B-V-1C, 2B-2C, 2B-3C, respectively. Finally, main flexural cracks occur with a significant deflection increase until failure. This flexibility is because of the development of the pressure diameter around the bolts. The pressure is controlled by three factors the GFRP thickness, the number, and the position of the bolts.

Nevertheless, with a change in diameter, the behavior changes slightly. After a sudden decrease in the applied load, it returns to rise again. The sharp reduction is noticed due to the instantaneous debonding in the pure bending section. Since the interface remained well-bonded to the end-anchor plate, the beam kept supporting the applied load. As it is further increases, the GFRP plate completely fails. The load shows a rapid fall like 4B-2C-D6, 8B-3C-D6, or a slowing down of the load with a substantial deflection rise like 4B-1C-D6, 8B-1C-D6, 8B-2C-D6. Because of the presence of the end anchor, the sample can continue to support the load.

Finally, the third type is presented with two peaks; the first peak of the load is about 98%, 166%, and 188% in beams 4B-V-2C, 4B-H-2C, 4B-V-3C, 4B-H-3C, 8B-1C, 8B-1C, 8B-2C, 8B-3C, respectively. The applied load increases again until the second peak due to the strength of the end-anchorage system. Then, the next sudden drop appears as the samples cannot allow the additional load. This sudden decrease is due to failure in the left or right part of the beam outside the reinforced area.

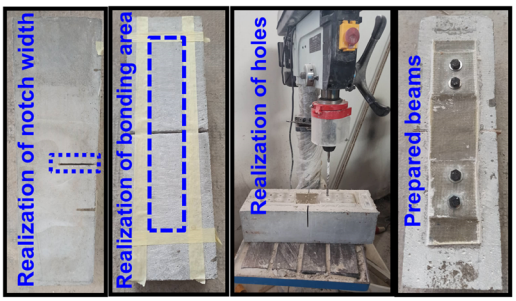

(a) Preparation steps

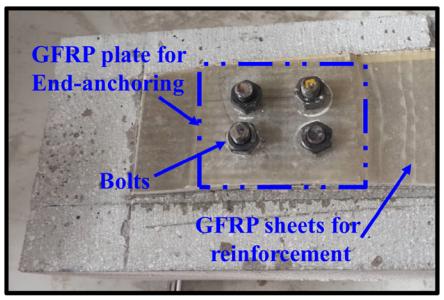

(b) Detail for anchorage GFRP

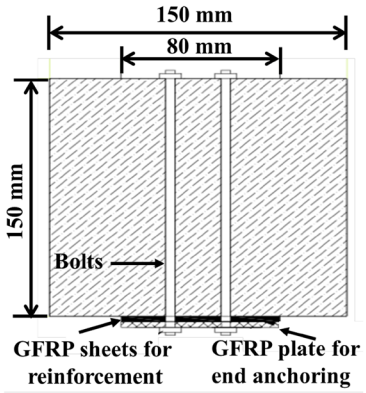

(c) Cross section of BGFPC beam

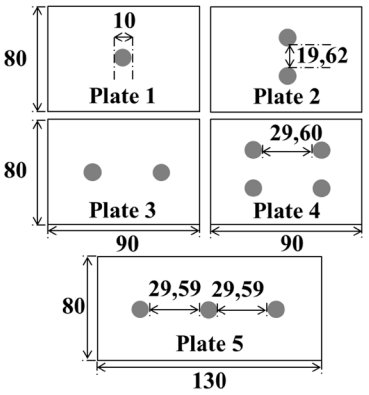

(d) GFRP plate for end-anchoring (all dimensions in mm)

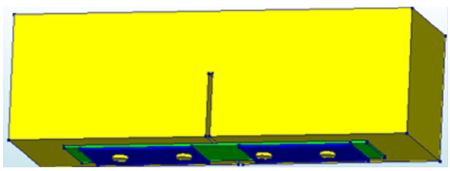

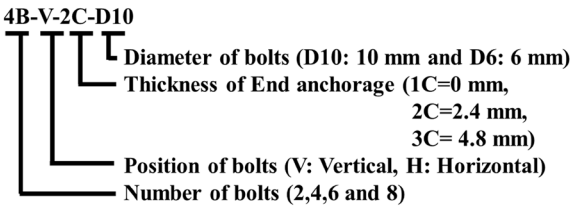

(e) Beam's designation and parameters of investigation

Fig. 2 Preparation of beams strengthened with bolt-glass fiber polymer composites (BGFPC)

3.2 Failure Mode and Cracking Pattern

Figs. 7 and 8 display pictures of below-reinforced beams strengthened with bolts-end anchoring GFRP composites (BEGFRPC) systems after failure. Different local and global failure modes include concrete cracks, crushing of GFRP plate, flexural damage, and shear cracks. The beam strengthened by bolts-end anchoring GFRP systems observed the debonding and delamination.

While under load, a sudden crack formed in the middle of the beam, which expanded rapidly with rising load until the glass FRP sheet debonded from one side of the notch. Fig. 7a shows the failure mode of the control beam (0B-1C); the flexural crack is developed at the mid-span in the maximum moment region. The maximum load capacity of this beam is about 23 kN, corresponding to a displacement of 0.5 mm.

Table 3 Technical details of the end-anchorages and the bolts

Specimen	End anchorage	Thickness of end-anchorage (mm)	Number of bolts	Position of bolts	Bolt diameter (mm)
B0-1C	Without	0	0	–	0
B2-1C-D10	Without	0	2	–	10
B4-H-1C-D10	Without	0	4	Horizontal	10
B4-H-1C-D6	Without	0	4	Horizontal	6
B4-V-1C-D10	Without	0	4	Vertical	10
B6-V-1C-D10	Without	0	6	Vertical	10
B8-H-1C-D10	Without	0	8	Horizontal	10
B8-H-1C-D6	Without	0	8	Horizontal	6
B2-2C-D10	With	2.4	2	Horizontal	10
B4-H-2C-D10	With	2.4	4	Horizontal	10
B4-H-2C-D6	With	2.4	4	Horizontal	6
B4-V-2C-D10	With	2.4	4	Vertical	10
B6-V-2C-D10	With	2.4	6	Vertical	10
B8-H-2C-D10	With	2.4	8	Horizontal	10
B8-H-2C-D6	With	2.4	8	Horizontal	6
B2-3C-D10	With	2.4	2	–	10
B4-H-3C-D10	With	4.8	4	Horizontal	10
B4-H-3C-D6	With	4.8	4	Horizontal	6
B4-V-3C-D10	With	4.8	4	Vertical	10
B6-V-3C-D10	With	4.8	6	Vertical	10
B8-H-3C-D10	With	4.8	8	Horizontal	10
B8-H-3C-D6	With	4.8	8	Horizontal	6

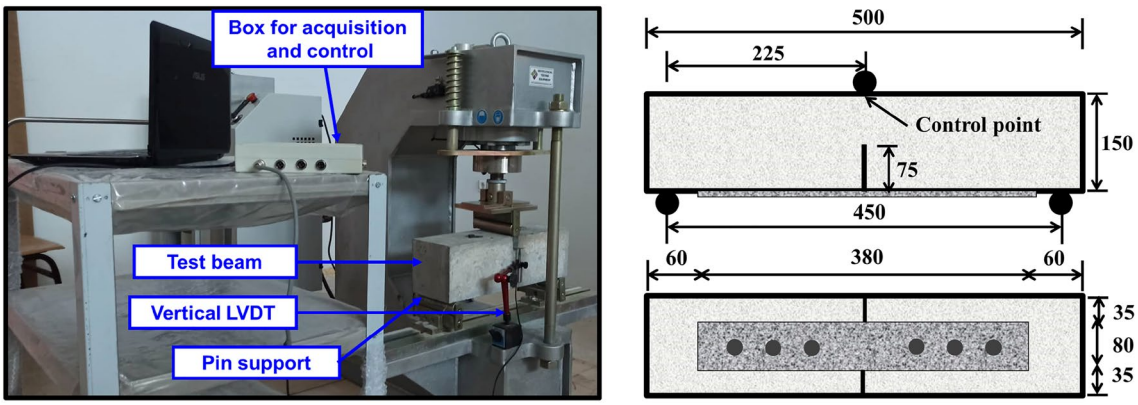

Fig. 3 Loading device and specimen dimension according to ASTM D7958/D7958M regulation (all dimensions in mm)

Figs. 7 and 8 display the failure modes for beams strengthened with bolts. The bolts' numbers, positions, and diameters have been investigated in this test. As displayed in Figs. 7b and 8a, the strengthened beams 2B-1C-D10, 4B-H-1C-D10, 4B-V-1C-D10, 6B-V-1C-D10, 4B-H-1C-D6, flexural cracks are initially formed in the maximum moment region and simultaneously anchoring plates remain attached to the bolts. This attachment allows the beams to resist new loads. With an increase in the applied load, a great diameter pressure on the bolts is developed, which leads to crashing in the GFRP plate after the second peak load. As a result, the load capacity decreases, and deflection increases until the typical ductile

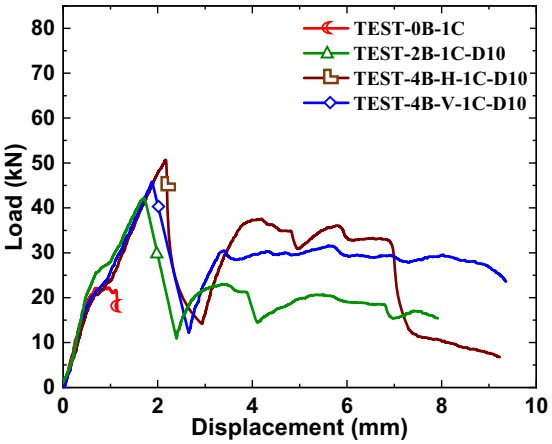

(a) Without using end anchorage GFRP

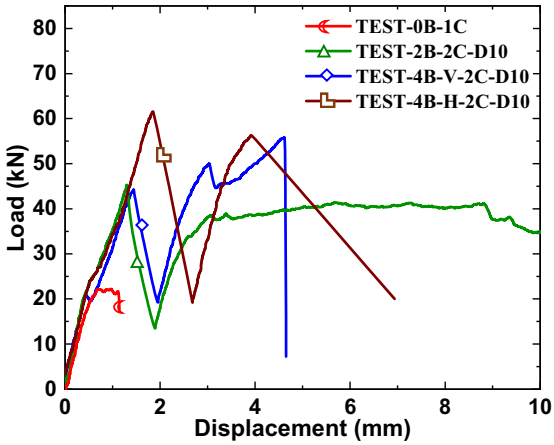

(b) End anchorage GFRP of 2.4 mm thickness

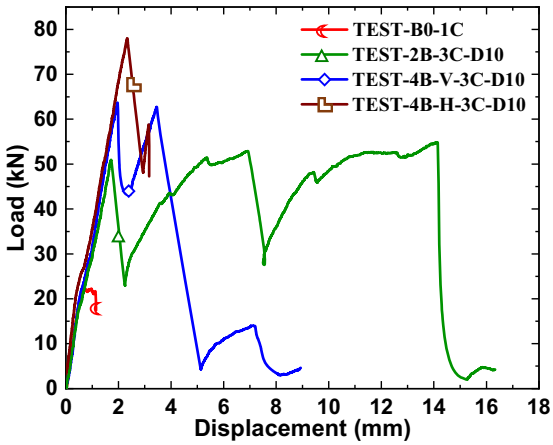

(c) End-anchorage GFRP of 4.8 mm thickness

Fig. 4 Typical load versus mid-span deflection curves with variation in position of bolts

flexural failure mode takes place. However, for beams 8B-1C-D10 and 8B-1C-D6, occurs near the last bolts leading to a shear failure mode.

The main failure modes in all BEGFRP beams of 2.4 and 4.8 mm thickness are initially flexural cracks at the mid-span. Then, the debonding occurs near the last bolts leading to a shear failure regardless of the position and diameter of the bolts.

In addition, the shear cracks always occur near the supports In addition, the shear cracks always occur near the supports, and then they propagate in different directions. For example: for a beam with a GFRP thickness of 2.4 mm and the number of bolts 2 or 4, the degree of inclination is greater than 60°, but for eight bolts, it is less than 60°. As for a beam with a GFRP thickness of 4.8 mm, the crack inclination angle for two bolts is greater than 60 degrees, but in the other cases, it is much less.

In addition, Figs. 7b–d and 8 show that beams strengthened with different bolts (in number, position, and diameter) do not have the same capacity and shape of failure. However, the interaction between the concrete and the glass FRP is reasonable due to the use of bolts.

3.3 Elastic Stiffness

Based on the previous load–deflection curves, Fig. 9a, b shows the values of the elastic stiffness (KE) obtained by evaluating the slope before the first appearance of the main flexural crack. For easy comparison, the elastic stiffness of the below-reinforced beams strengthened with bolt-glass fiber polymer composites (BGFPC) is normalized against the control beam. It is noticed that without end-anchorage GFRP, the elastic stiffness is not improved, whatever the bolts quantity used. Furthermore, the influence of the thickness of end-anchorage

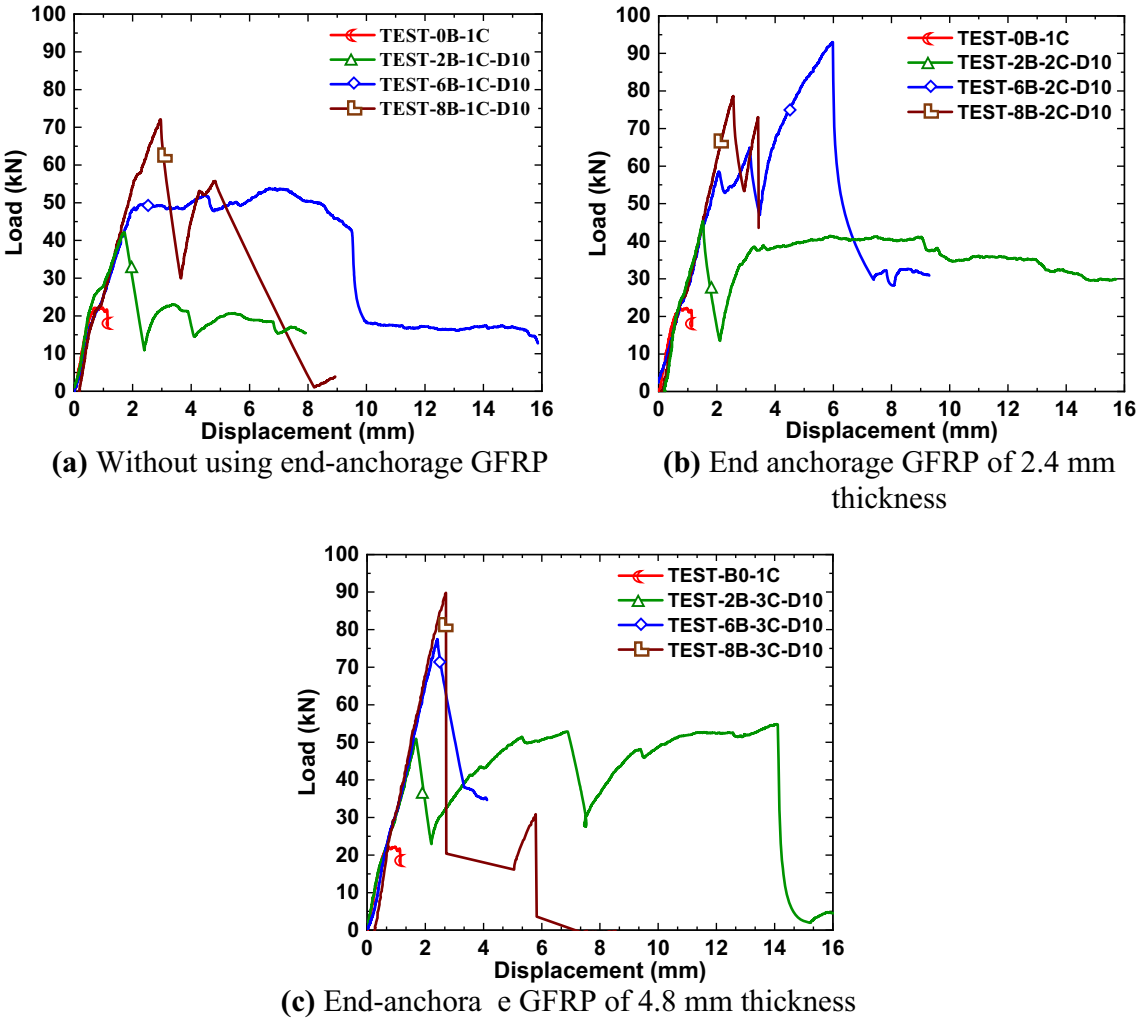

Fig. 5 Typical load versus mid-span deflection curves with variation in number of bolts

GFRP on elastic stiffness (KE) is relatively limited. For example, the enhancement in (KE) when using four horizontal bolts is 1.3 (30%) and 1.27 (27%) for end-anchorage GFRP thickness of 2.4 mm and 4.8 mm, respectively. However, these percentages are, respectively, 44% and 41% more than that obtained without end-anchorage GFRP. Therefore, end-anchorage GFRP is too necessary for such reinforcement. The optimal thickness of the end-anchorage GFRP will be determined after analyzing figures related to the ultimate flexural load and the energy absorption.

The effect of bolt diameter and end-anchorage thickness on the normalized elastic stiffness of the beams strengthened with (BGFPC) is shown in Fig. 10a, b using 4 and 8 bolts, respectively. As can be seen, added glass fiber polymer composites with intermediate and high thickness cause an increase in the elastic stiffness of the beams. In addition, bolts of 10 mm in diameter are mainly sufficient to obtain relatively high elastic stiffness. The values of the elastic stiffness obtained from the load–deflection relationship are given in Table 4.

3.4 Ultimate Loads and Flexural Capacity

Fig. 11a, b provides the ultimate loads of the below-reinforced beams strengthened with (BGFPC). In general, the force that creates failure in the beam is increased by increasing the bolt quantity and the thickness of the anchorage GFRP. Six bolts with a GFRP of 2.4 mm are

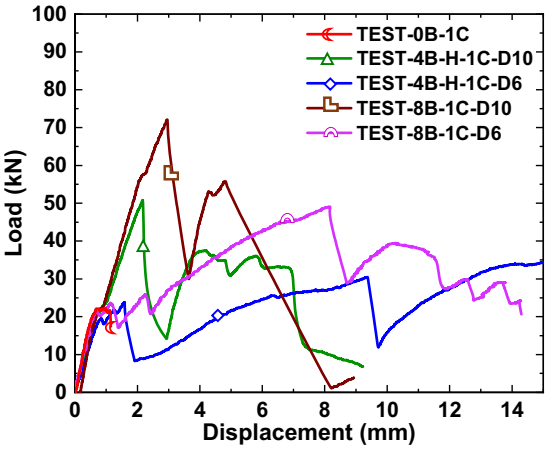

(a) Without using end-anchorage GFRP

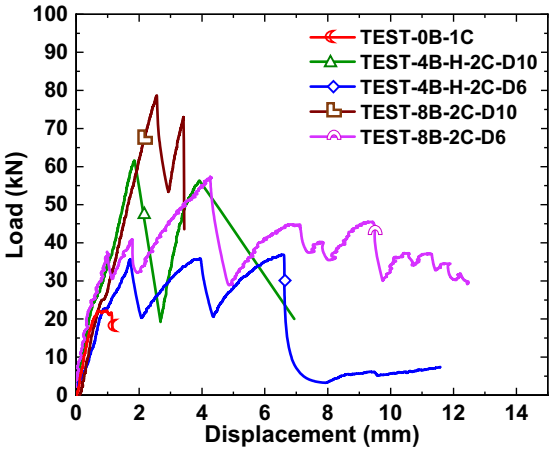

(b) End-anchorage GFRP of 2.4 mm thickness

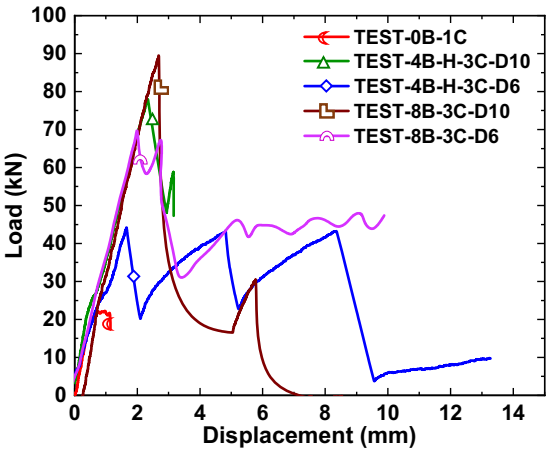

(c) End-anchorage GFRP of 4.8 mm thickness

Fig. 6 Typical load versus mid-span deflection curves with variation in diameter of bolt

mainly sufficient to obtain relatively high ultimate loads. In addition, in the case of using four horizontal bolts, it is necessary to increase the thickness of the anchorage GFRP to 4.8 mm.

Figs. 11a and b provide the ultimate loads of the below-reinforced beams strengthened with (BGFPC) using 4 and 6–8 bolts, respectively.

Figs. 12a and b shows the effect of bolt diameter and end-anchorage thickness on the normalized ultimate load of the strengthened beams using 4 and 8 bolts, respectively. It is noticed that the bolts of 10 mm in diameter give a high ultimate load, whatever their quantity. The values of the ultimate load obtained from the load-deflection relationship are shown in Table 4.

3.5 Energy Absorption Capacity

The energy absorption (EA) of all beams strengthened with bolt-glass fiber polymer composites (BGFPC) is represented in Fig. 13a, b. This energy is obtained by finding the area under a load-displacement curve. The EA has been normalized against the control beam for easy comparison, as illustrated in Fig. 13a, b. In addition, the energy absorptions before and after peak cracking are shown in Fig. 13c, d. Inspection of these figures reveals that the energy absorption values are maximal for beams reinforced with only two bolts. However, the previous results illustrated in Fig. 11a, b showed that the ultimate load corresponding to this configuration is relatively limited. Therefore, the reinforced beams strengthened with

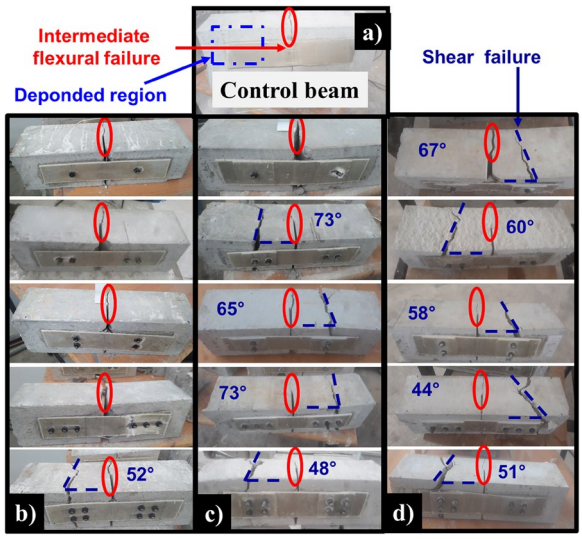

Fig. 7 Typical failure modes for beams strengthened with bolt (diameter 10 mm)-glass fiber polymer composites (BGFPC) systems: **a** control beam; **b** without using end-anchorage GFRP; **c** end anchorage GFRP of 2.4 mm thickness; **d** end-anchorage GFRP of 4.8 mm thickness

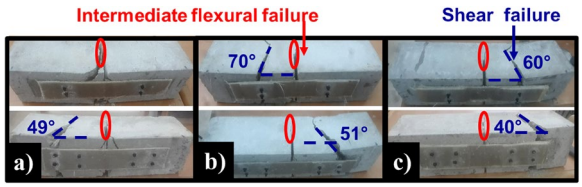

Fig. 8 Typical failure modes for beams strengthened with bolt (Diameter 6 mm)-glass fiber polymer composites (BGFPC) systems: **a** without using end-anchorage GFRP; **b** end-anchorage GFRP of 2.4 mm thickness; **c** end-anchorage GFRP of 4.8 mm thickness

six bolts and end-anchorage GFRP of 2.4 mm thickness could be considered as the optimal configuration for such reinforcement. This choice is also confirmed based on Fig. 7c, in which the strengthened beam with six bolts and end-anchorage GFRP of 2.4 mm thickness has the highest angle of shear crack, 73°. This orientation confirms that the bolts tend to be involved in the reinforcement mechanism.

The effect of bolt diameter and end-anchorage thickness on the normalized energy absorption of the below-reinforced beams strengthened with bolt-glass fiber composites (BGFPC) is shown in Fig. 14a, b using 4 and 8 bolts, respectively. In addition, the energy absorptions before and after peak cracking are shown in Fig. 14c, d. In general, the added end-anchoring glass fiber polymer composites with bolts of 6 mm largely increase the energy absorption of the beams. Therefore, combining bolts with diameters of 6 and 10 mm would be the best solution for increasing the ultimate load and the ductility of the beams. The values of the energy absorption obtained from the load-deflection relationship are given in Table 4.

The energy absorptions before and after peak cracking are also shown in Table 4. It is observed that the control beam without end anchor GFRP plates has the lowest pre-cracking energy absorption value. The pre-cracking energy absorption increases significantly with increasing the thickness of the glass fiber polymer composites. On the other hand, the highest energy absorption value after cracking is obtained for beams strengthened with two bolts and 2.4 mm thick anchor GFRP plates. In anthor research (), it is conluded that AE activity is about 20-30% more in GFRP-RC beams as compared to steel-RC beams.

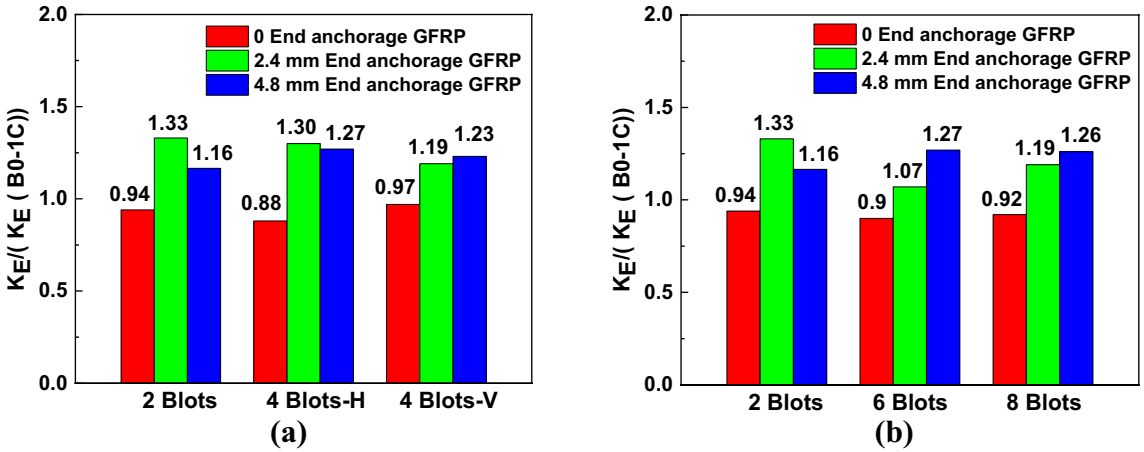

Fig. 9 Normalized elastic stiffness versus bolt quatity (diameter 10 mm) and end-anchorage thickness

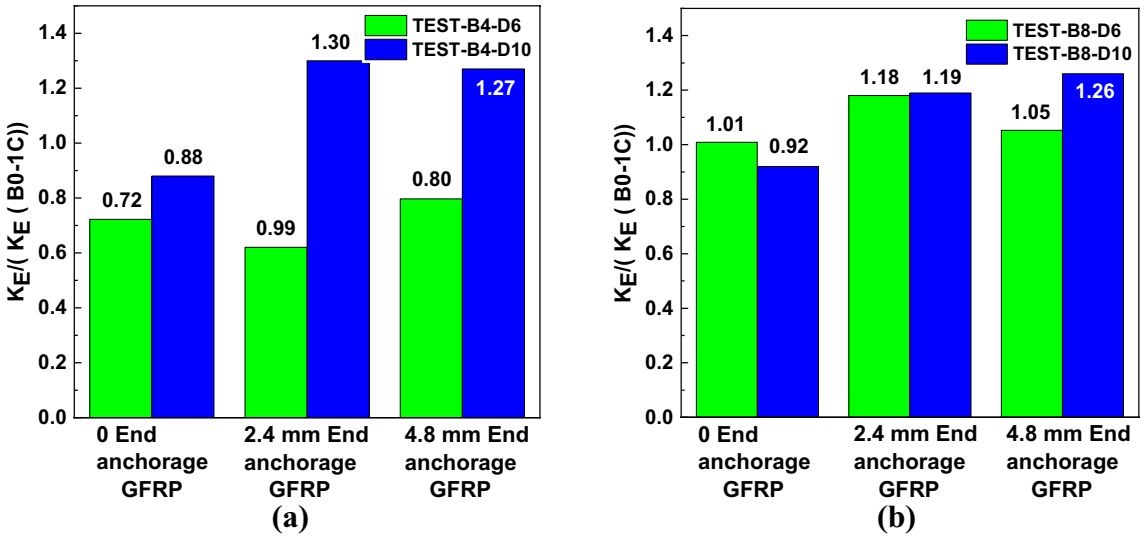

Fig. 10 Normalized elastic stiffness versus bolt diameter and end anchorage thickness

Table 4 Results of ultimate load, elastic stiffness and energy absorption of beams strengthened with bolt-glass fiber polymer composites (BGFPC)

Specimen	P_u (kN)	KE (kN/mm)	Pre-cracking EA (kN.mm)	Post-cracking EA (kN.mm)	Total EA (kN.mm)
B0-1C	22.59	26.27	11.04	7.52	18.56
B2-C1-D10	42.05	24.74	61.33	103.37	164.7
B4-H-C1-D10	50.78	23.29	74.16	157.07	231.23
B4-H-C1-D6	34.03	24.73	29.11	531.73	560.84
B4-V-C1-D10	46.02	25.57	69.07	190.52	259.59
B6-V-C1-D10	53.8	23.57	67.16	467.64	534.8
B8-H-C1-D10	72.32	24.19	145.47	148.53	294
B8-H-C1-D6	49.05	34.53	23.15	442.95	466.1
B2-C2-D10	45.31	35.12	47.92	492.42	540.34
B4-H-C2-D10	61.57	34.21	95.55	167.59	263.14
B4-H-C2-D6	36.77	21.24	42.44	143.07	185.51
B4-V-C2-D10	56.4	31.20	51.12	120.83	171.95
B6-V-C2-D10	93.54	28.21	73.56	376.24	449.8
B8-C2-D10	78.86	31.17	79.50	73.76	153.26
B8-H-C2-D6	57.35	40.40	28.32	447.79	476.11
B2-C3-D10	50.8	30.60	64.20	558.33	622.53
B4-H-C3-D10	77.47	33.25	135.74	12.59	148.33
B4-H-C3-D6	44.45	27.27	54.56	317.7	372.26
B4-V-C3-D10	64.17	32.41	84.83	137.3	222.13
B6-V-C3-D10	77	33.33	118.78	54.1	172.88
B8-H-C3-D10	89 0.7	33.22	161.59	21.13	182.72
B8-H-C3-D6	71.97	39.03	92.33	316.02	408.35

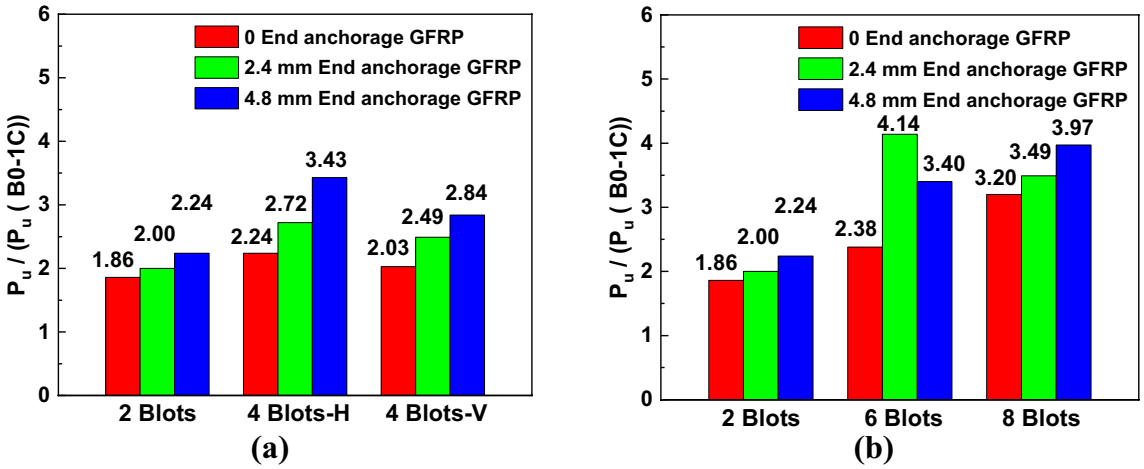

Fig. 11 Normalized ultimate load versus bolt quatity (diameter 10 mm) and end-anchorage thickness

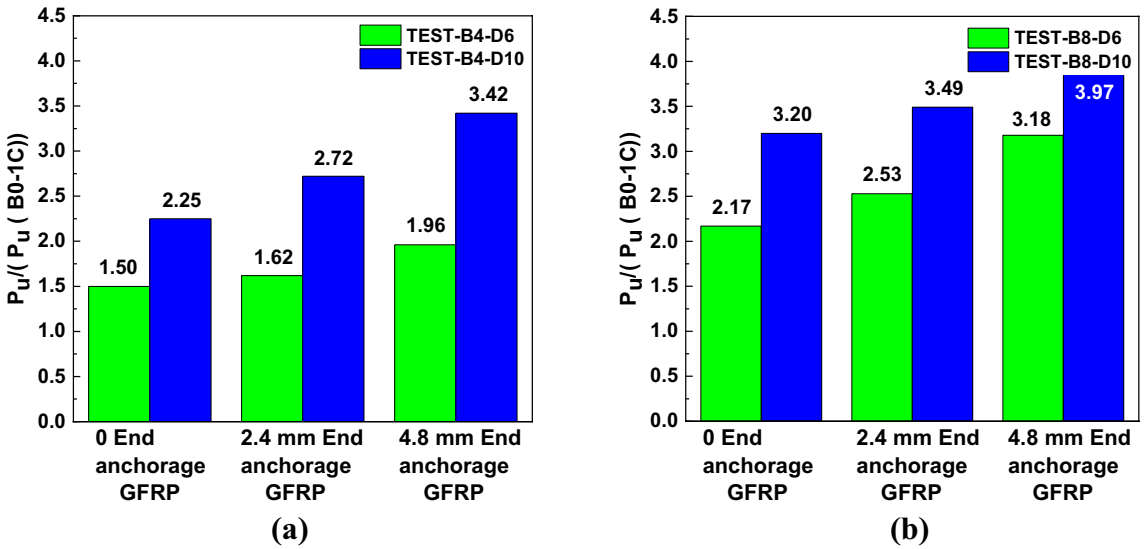

Fig. 12 Normalized ultimate load versus bolt diameter and end-anchorage thickness

4 Conclusion

This research investigates the bending response behavior of below-reinforced beams strengthened with bolt-end-anchoring glass fiber polymer composites (BEGFRPC) subjected to quasi-static loads. The experimental results provide a comprehensive database to predict the structural responses of BEGFPC subjected to bending.

On one hand, the typical load-deflection relationships are divided into three types of responses. Initially, the first type is described in specimen 0B-1C. When the load increases linearly up to 23 kN, it drops sharply, because the interface is deboning to the beam. The second type presents a substantial augmentation in the applied load; of about 90%, 104%, and 127% in beams 2B-1C-D10, 4B-H-1C-D10, 4B-V-1C-D10, 2B-2C-D10 and 2B-3C-D10, respectively. Afterward, the load suddenly decreases. This drop is because the GFRP sheet separates from the beam in the middle. Finally, the third type is presented with two peaks; the first peak of load about 98%, 166%, and 188% in beams 4B-V-2C, 4B-H-2C,

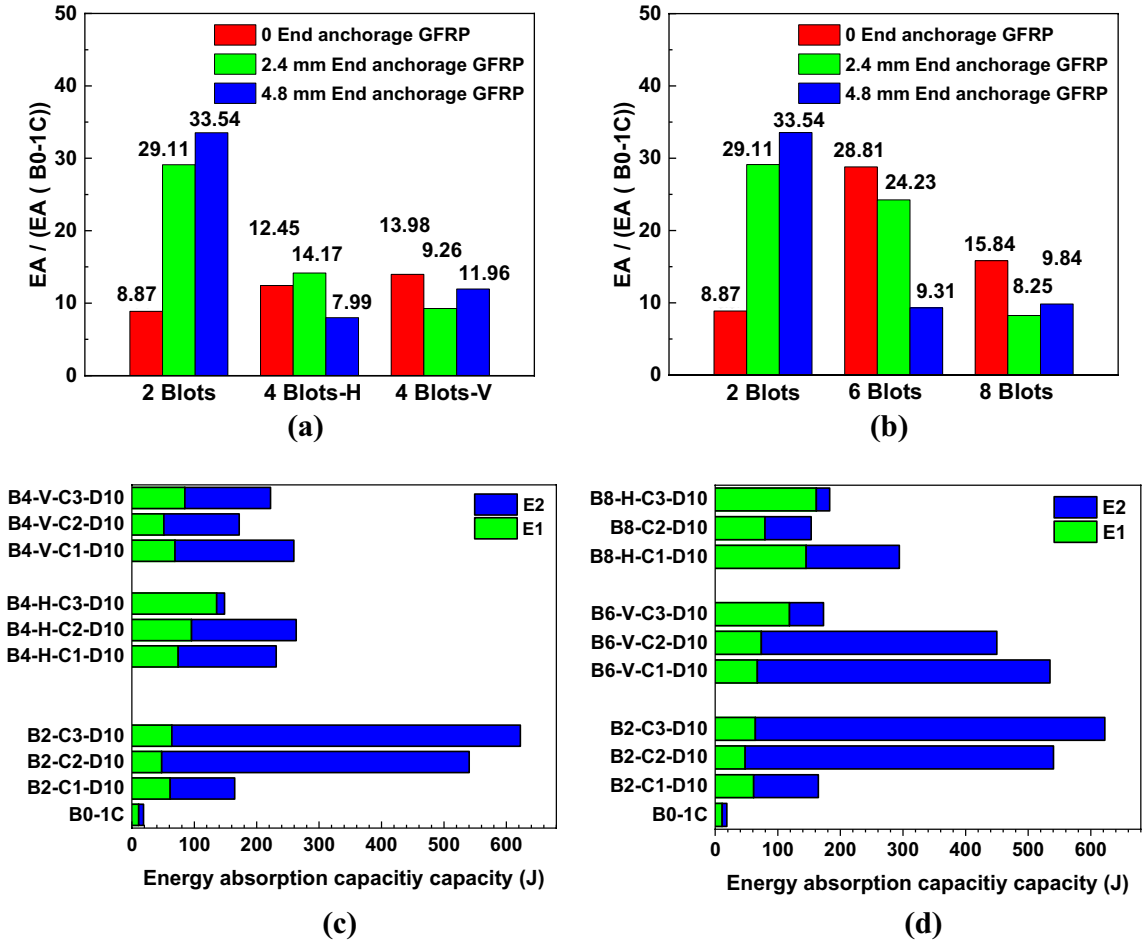

Fig. 13 Energy absorption versus bolt quatity (diameter 10 mm) and end-anchorage thickness: **a**, **b** normalized values; **c**, **d** detail of pre (E1) and post (E2)-energy absorption

4B-V-3C, 4B-H-3C, 8B-1C, 8B-1C, 8B-2C, 8B-3C, respectively. The next sudden drop appears as the beams cannot allow the additional load. This sudden decrease is due to failure in the left or right part of the beam outside the reinforced area.

On the other hand, the beams strengthened with six bolts and end-anchorage GFRP of 2.4 mm thickness had shown a significant deformation before failure, higher energy absorption capacity with lower stiffness than control beams. In addition, such beams have the most increased shear crack angle, 73°. This orientation confirmed that the bolts tend to be involved in the reinforcement mechanism.

The present findings will be adopted in numerical simulations of time-consuming experiments of RC structures subjected to bending loading.

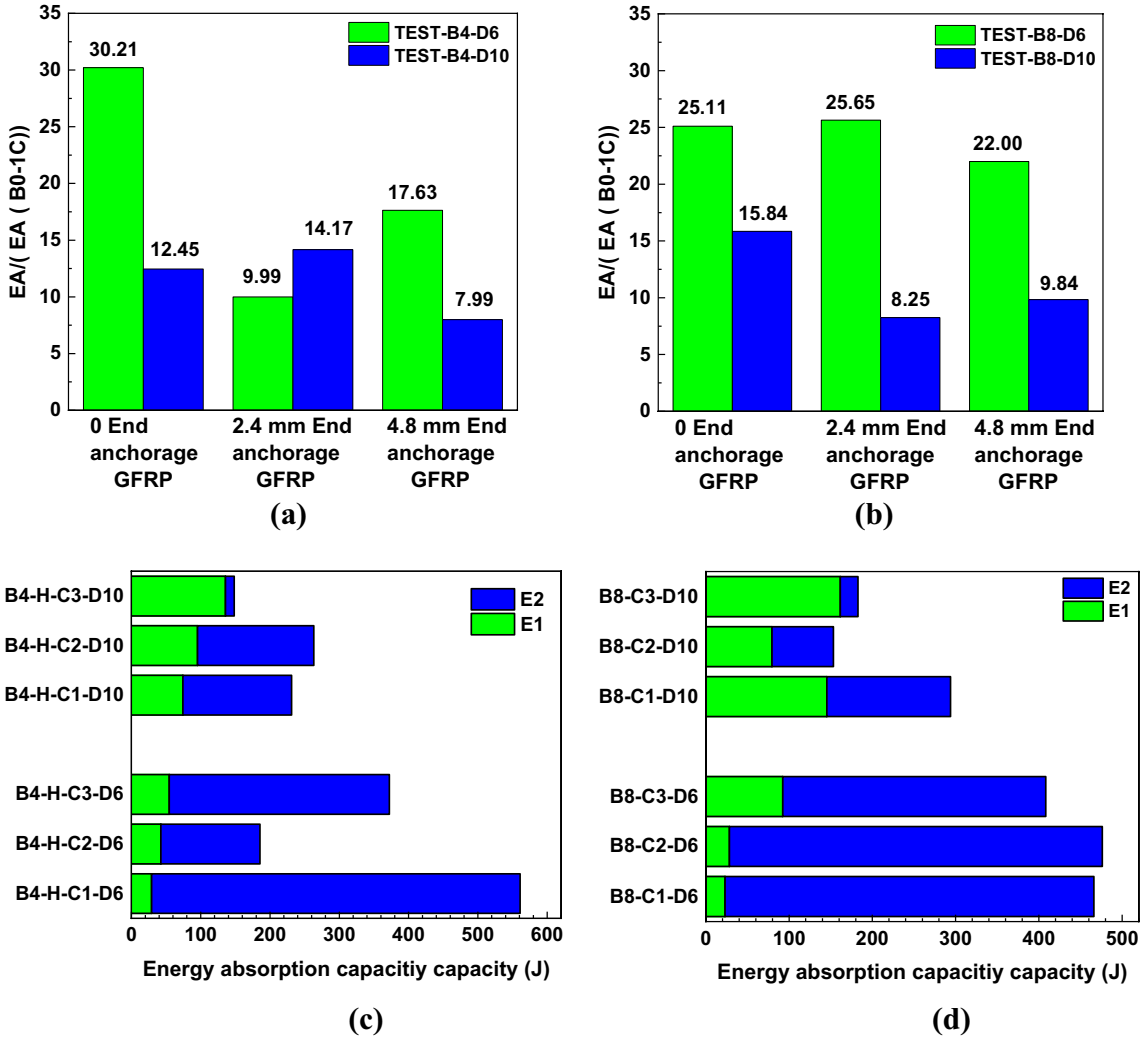

Fig. 14 Energy absorption versus bolt diameter and end-anchorage thickness: **a**, **b** normalized values; **c**, **d** detail of pre (E1) and post (E2)-energy absorption

Author contributions
All authors read and approved the final manuscript.

Author's information
Djarir Yahiaoui: First Author and corresponding Author, Associate Professor at the Department of Civil Engineering, Faculty of Technology, University of Batna 2, Algeria. Abdelaziz Boutrid: Second Author, Associate Professor at the Department of Civil Engineering, Faculty of Science and Technology, Abbès Laghrour University, Khenchela, Algeria. Mohamed Saadi: Third Author, Ph.D at the Department of Civil Engineering, Faculty of Technology, University of Batna 2, Algeria. Belgacem Mamen: Fourth Author, Associate Professor at the Department of Civil Engineering, Faculty of Science and Technology, Abbès Laghrour University, Khenchela, Algeria. Tayeb Bouzid: Fifth Author, senior researcher at the Laboratory *LGC-ROI*, University of Batna 2, Algeria.

Availability of data and materials
The data sets used and/or analyzed during the current study are available from the corresponding author on reasonable request.

Declarations

Competing interests
The authors declare that they have no competing interests.

Received: 5 September 2022 Accepted: 4 January 2023
Published online: 23 March 2023

References

A.C. Institute. (2008). Guide for the design and construction of externally bonded FRP systems for strengthening concrete structures, In *ACI 440.2 R-08, American Concrete Institute*.

ACI 211.1–Reapproaved 2009. (2009). Standard practice for selecting proportions for normal, heavyweight, and mass concrete, *An ACI Standard Reported by ACI Committee 211* (p. 38).

Alasadi, S., Ibrahim, Z., Shafigh, P., Javanmardi, A., & Nouri, K. (2019). An experimental and numerical study on the flexural performance of over-reinforced concrete beam strengthening with bolted-compression steel plates: Part II. *Applied Sciences, 10*(1), 94. https://doi.org/10.3390/app10010094

Al-Hamrani, A., & Alnahhal, W. (2021). Shear behavior of basalt FRC beams reinforced with basalt FRP bars and glass FRP stirrups: Experimental and analytical investigations. *Engineering Structures, 242*, 112612. https://doi.org/10.1016/j.engstruct.2021.112612

Ali, H. M., Sheikh, M. N., & Hadi, M. N. (2022). Flexural strengthening of RC beams with NSM-GFRP technique incorporating innovative anchoring system. *Structures, 38*, 251–264. https://doi.org/10.1016/j.istruc.2022.01.088

AminiPishro, A., Zhang, S., Zhang, Z., Zhao, Y., AminiPishro, M., Zhang, L., & Postel, V. (2022a). Structural behavior of FRP-retrofitted RC beams under combined torsion and bending. *Materials, 15*(9), 3213. https://doi.org/10.3390/ma15093213

AminiPishro, A., Zhang, Z., AminiPishro, M., Liu, W., Zhang, L., & Yang, Q. (2022b). Structural performance of EB-FRP-strengthened RC T-beams subjected to combined torsion and shear using ANN. *Materials, 15*(14), 4852. https://doi.org/10.3390/ma15144852

ASTM. (2010). *D638–10 Standard test method for tensile properties of plastics*. American Society for Testing and Materials.

ASTM. (2017). *Standard test method for evaluation of performance for FRP composite bonded to concrete substrate using beam test; ASTM D7958/D7958M*. ASTM.

ASTM C39/C39M-17b. (2017). *Standard test method for compressive strength of cylindrical concrete specimens*. ASTM International.

Chen, C., Cheng, L., Sui, L., Xing, F., Li, D., & Zhou, Y. (2018a). Design method of end anchored FRP strengthened concrete structures. *Engineering Structures, 176*, 143–158. https://doi.org/10.1016/j.engstruct.2018.08.081

Chen, W., Pham, T. M., Sichembe, H., Chen, L., & Hao, H. (2018b). Experimental study of flexural behaviour of RC beams strengthened by longitudinal and U-shaped basalt FRP sheet. *Composites Part B Engineering, 134*, 114–126. https://doi.org/10.1016/j.compositesb.2017.09.053

Del Rey Castillo, E., Griffith, M., & Ingham, J. (2018). Seismic behavior of RC columns flexurally strengthened with FRP sheets and FRP anchors. *Composite Structures, 203*, 382–395. https://doi.org/10.1016/j.compstruct.2018.07.029

Djeddi, F., Ghernouti, Y., Abdelaziz, Y., & Alex, L. (2016). Strengthening in flexure–shear of RC beams with hybrid FRP systems: Experiments and numerical modeling. *Journal of Reinforced Plastics and Composites, 35*(22), 1642–1660. https://doi.org/10.1177/0731684416662532

El Ghadioui, R., Wagner, J., Klein, J., Proske, T., Curbach, M., & Graubner, C. A. (2022). RC members with a flexural-strengthening layer of CFRP textile-reinforced concrete under monotonic and cyclic long-term loading. *Structural Concrete, 23*(2), 939–953. https://doi.org/10.1002/suco.202100452

Esmaeili, J., Aghdam, O. R., Andalibi, K., Kasaei, J., & Gencel, O. (2022). Experimental and numerical investigations on a novel plate anchorage system to solve FRP debonding problem in the strengthened RC beams. *Journal of Building Engineering, 45*, 103413. https://doi.org/10.1016/j.jobe.2021.103413

Garhwal, S., Sharma, S., & Sharma, S. K. (2021). Monitoring the flexural performance of GFRP repaired corroded reinforced concrete beams using passive acoustic emission technique. *Structural Concrete, 22*(1), 198–214. https://doi.org/10.1002/suco.202000247

Mhanna, H. H., Hawileh, R. A., & Abdalla, J. A. (2021, December). Effect of FRP Anchor Inclination Angle on Shear Strengthening of Reinforced Concrete T-beams. In International Conference on Fibre-Reinforced Polymer (FRP) Composites in Civil Engineering (pp. 2169–2179). Springer. https://doi.org/10.1007/978-3-030-88166-5_187

Nguyen, H., Mutsuyoshi, H., & Zatar, W. (2015). Hybrid FRP-UHPFRC composite girders: Part 1–experimental and numerical approach. *Composite Structures, 125*, 631–652. https://doi.org/10.1016/j.compstruct.2014.10.038

Nili, M., Sasanipour, H., & Aslani, F. (2019). The effect of fine and coarse recycled aggregates on fresh and mechanical properties of self-compacting concrete. *Materials, 12*(7), 1120. https://doi.org/10.3390/ma12071120

NoroozOlyaee, M., & Mostofinejad, D. (2019). Slenderness effects in circular RC columns strengthened with CFRP sheets using different external bonding techniques. *Journal of Composites for Construction, 23*(1), 04018068. https://doi.org/10.1061/(ASCE)CC.1943-5614.0000908

Pavithra, C., Revathy, J., & Gajalakshmi, P. (2022). Structural behavior of hybrid double-skin tubular FRP–concrete–steel column: State-of-the-art review. *Innovative Infrastructure Solutions, 7*(1), 1–19. https://doi.org/10.1007/s41062-021-00653-3

Pishro, A. A., & Feng, X. (2017). RC beams behavior retrofitted by FRP subjected to torsion, shear and flexure-a review. *International Journal of Computer Science and Network Security (IJCSNS), 17*(2), 34.

Salama, A. S. D., Hawileh, R. A., & Abdalla, J. A. (2019). Performance of externally strengthened RC beams with side-bonded CFRP sheets. *Composite Structures, 212*, 281–290. https://doi.org/10.1016/j.compstruct.2019.01.045

Sankaramoorthy, T., Karthikeyan, R., Pradeep, G. M., Athikesavan, D., & Girimurugan, R. (2022). Improved performance of confinement of RC beam with glass fibre reinforced polymer laminates. *Materials Today: Proceedings, 56*, 3190–3195. https://doi.org/10.1016/j.matpr.2021.09.280

Sharma, G., Sharma, S., & Sharma, S. K. (2022). Monitoring structural behaviour of concrete beams reinforced with steel and GFRP bars using acoustic emission and digital image correlation techniques. *Structure and Infrastructure Engineering, 18*(2), 167–182. https://doi.org/10.1080/15732479.2020.1836661

Tran, Q. D., Nhut, P. V., & Matsumoto, Y. (2022). Multi-bolted connection for pultruded glass fiber reinforced polymer's structure: A study on strengthening by multiaxial glass fiber sheets. *Polymers, 14*(8), 1561. https://doi.org/10.3390/polym14081561

Tudjono, S., Lie, H. A., & Hidayat, B. A. (2015). An experimental study to the influence of fiber reinforced polymer (FRP) confinement on beams subjected to bending and shear. *Procedia Engineering, 125*, 1070–1075. https://doi.org/10.1016/j.proeng.2015.11.164

Vahidpour, M., Kheyroddin, A., & Kioumarsi, M. (2022). Experimental investigation on flexural capacity of reinforced concrete beams strengthened with 3D-fiberglass, CFRP and GFRP. *International Journal of Concrete Structures and Materials, 16*(1), 1–20. https://doi.org/10.1186/s40069-022-00508-w

Yahiaoui, D., Saadi, M., & Bouzid, T. (2022). Compressive behavior of concrete containing glass fibers and confined with glass FRP composites. *The International Journal of Concrete Structures and Materials, 16*(1), 1–19. https://doi.org/10.1186/s40069-022-00525-9

Zhang, S. S., Ke, Y., Smith, S. T., Zhu, H. P., & Wang, Z. L. (2021). Effect of FRP U-jackets on the behaviour of RC beams strengthened in flexure with NSM CFRP strips. *Composite Structures, 256*, 113095. https://doi.org/10.1016/j.compstruct.2020.113095

Zhou, Y., Chen, X., Fan, Z., Sui, L., Li, D., & Xing, F. (2017). Bond behaviors of FRP-to-concrete interface under the control of a novel end-anchorage system. *Composite Structures, 168*, 130–142. https://doi.org/10.1016/j.compstruct.2017.02.056

Zhou, Y., Wang, X., Sui, L., Xing, F., Wu, Y., & Chen, C. (2018). Flexural performance of FRP-plated RC beams using H-type end anchorage. *Composite Structures, 206*, 11–21. https://doi.org/10.1016/j.compstruct.2018.08.015

Publisher's Note

Springer Nature remains neutral with regard to jurisdictional claims in published maps and institutional affiliations.

Submit your manuscript to a SpringerOpen journal and benefit from:

- ► Convenient online submission
- ► Rigorous peer review
- ► Open access: articles freely available online
- ► High visibility within the field
- ► Retaining the copyright to your article

Submit your next manuscript at ► springeropen.com